

Tails for the Einstein-Yang-Mills system

Michael Pürrer and Peter C Aichelburg

Institut für Theoretische Physik, Universität Wien, 1090 Wien, Austria

E-mail: Michael.Puerrerr@univie.ac.at,
Peter.Christian.Aichelburg@univie.ac.at

Abstract. We study numerically the late-time behaviour of the coupled Einstein Yang-Mills system. We restrict ourselves to spherical symmetry and employ Bondi-like coordinates with radial compactification. Numerical results exhibit tails with exponents close to -4 at timelike infinity i^+ and -2 at future null infinity \mathcal{I}^+ .

PACS numbers: 04.25.D-, 04.40.Nr, 03.65.Pm, 02.70.Bf

1. Introduction

Radiating systems relax to equilibrium by dissipating energy to infinity. The fall-off properties of the field at late times are governed by so-called radiation tails. These tails emerge from primary outgoing radiation that is backscattered. This far-field effect is either due to a background or an effective potential produced by the nonlinearities of the radiation field itself, or in general, a mixture of both.

The classical fall-off properties were based on linear perturbations about a given background [1]. However, Bizon [2] has shown, that for certain nonlinear systems the nonlinear tails may dominate the long-time behaviour, i.e. these tails fall off more slowly in time than the linear perturbations. As an example, he studied the spherically symmetric Yang-Mills equations on Minkowski and Schwarzschild spacetimes [3]. While linear perturbation theory predicts a t^{-5} power law decay due the backscattering off the Schwarzschild curvature, the nonlinear part decays only as t^{-4} for observers near timelike infinity. This slower fall-off was also observed numerically. More recently, these results were confirmed and extended to the late-time behaviour at future null infinity by Zenginoğlu [4], showing that tails die off as t^{-2} on Schwarzschild spacetime.

These calculations are on a given background and the question arises what happens for the coupled Einstein-Yang-Mills system. In the fully coupled case it is difficult to disentangle the different contributions. If one writes down a perturbation expansion starting from flat spacetime, then the first order perturbation of the YM field evolves in an effective potential produced by the back reaction of the YM-field to the metric. In addition, there will be the nonlinear effects from the YM equation already present in flat space. In this sense all tails are nonlinear, however, it is not evident what the overall fall-off behaviour is. The aim of this paper is to answer this question numerically.

It is known that the possible stable endstates of (spherically symmetric) collapse for the Einstein-YM system are either the formation of a black hole or dispersion to flat space. Black holes come in two types: pure black holes, i.e. with all of the YM field radiated away or coloured [5]. In addition, there exist soliton solutions found by Barnik and McKinnon [6]. However, both solitons and colored black holes turned out to be unstable under linear perturbations. For technical reasons we restrict ourselves to subcritical evolutions which do not form black holes. However, from the results in [3, 4], we expect our findings to hold also for generic spherically symmetric initial data when a black hole is formed.

We tackle this problem by numerically solving a characteristic initial value problem with constraints and employ radial compactification to allow investigation of tails at future null infinity. First we present the model, derive the equations of motion and write the Yang-Mills wave equation as an advection equation plus a constraint. Second, we discuss the numerical methods used for solving the given system and check the convergence of the code. Finally, we present results for late-time tails on Minkowski background and for the coupled Einstein-Yang-Mills system.

2. Model

We assume spherical symmetry with a regular center and choose Bondi-like coordinates $\{u, r, \theta, \phi\}$ based upon outgoing null hypersurfaces $u = \text{const}$ with the line-element [7]

$$ds^2 = -e^{2\beta(u,r)} \frac{V(u,r)}{r} du^2 - 2e^{2\beta(u,r)} du dr + r^2 d\Omega^2. \quad (1)$$

We consider the Yang-Mills theory with the gauge group $SU(2)$ and assume the magnetic ansatz for the gauge connection [3, 8]

$$A = w\tau^\theta d\theta + (\cot\theta\tau^r + w\tau^\phi) \sin\theta d\phi, \quad (2)$$

where $w = w(u, r)$ is the Yang-Mills field and the τ^a are the spherical generators of $su(2)$, normalized such that $[\tau^a, \tau^b] = i\epsilon^{abc}\tau^c$, where $a, b, c \in \{r, \theta, \phi\}$. They are related to the Pauli matrices σ^a via $\tau^a = \sigma^a/2$.

The Yang-Mills field strength (or curvature), $F = dA + A \wedge A$, then becomes

$$F = (\dot{w}du + w'dr) \wedge (\tau^\theta d\theta + \tau^\phi \sin\theta d\phi) - (1 - w^2) \tau^r d\theta \wedge \sin\theta d\phi, \quad (3)$$

where \dot{w} and w' denote partial derivatives of $w(u, r)$ with respect to u and r , respectively. Using the above ansatz the trace of the Yang-Mills curvature becomes

$$\text{tr}(F^{\mu\nu}F_{\mu\nu}) = F_{\mu\nu}^a F^{a\mu\nu} = -2\frac{e^{-2\beta}}{r^2} \left[2\dot{w}w' - \frac{V}{r}(w')^2 \right] + \frac{(1 - w^2)^2}{r^4}, \quad (4)$$

where Greek indices range over the four spacetime dimensions and Latin indices are group indices. The action for the Yang-Mills field coupled to Einstein's equations is [8]

$$S = \int d^4x \sqrt{-g} \left[\frac{R}{16\pi G} - \frac{1}{e^2} F_{\mu\nu}^a F^{a\mu\nu} \right], \quad (5)$$

The Yang-Mills wave equation is obtained by varying the action with respect to the Yang-Mills field w

$$-2\dot{w}' + \left(\frac{V}{r}\right)' w' + \frac{V}{r} w'' + \frac{e^{2\beta}}{r^2} w(1-w^2) = 0, \quad (6)$$

while variation with respect to the metric functions, β and V , yields two constraint equations

$$V' = e^{2\beta} \left[1 - \frac{8\pi G}{e^2} \frac{(1-w^2)^2}{r^2} \right] \quad (7)$$

$$\beta' = \frac{8\pi G}{e^2} \frac{(w')^2}{r}. \quad (8)$$

The coupling constant $[G/e^2]$ has dimension of *length*². Since it is not dimensionless, changing the coupling constant does not give rise to a one-parameter family of theories, but only changes the scale. To simplify the equations, we choose

$$\frac{8\pi G}{e^2} = 1. \quad (9)$$

The final form of the hypersurface equations then becomes

$$V' = e^{2\beta} \left[1 - \frac{(1-w^2)^2}{r^2} \right] \quad (10)$$

$$\beta' = \frac{(w')^2}{r}. \quad (11)$$

The regularity condition to be imposed on the Yang-Mills field at the origin is

$$w = \pm 1 + O(r^2) \quad (12)$$

while the gauge (u is chosen to be proper time at the regular center) and regularity conditions on the metric functions are

$$\beta = O(r^2) \quad (13)$$

$$V/r = 1 + O(r^2). \quad (14)$$

For the study of tail behaviour it is crucial to introduce a new field variable

$$\bar{w} := w - 1 \quad (15)$$

as a perturbation of one of the Yang-Mills vacua $w = \pm 1$, (i.e. where the field strength vanishes), in order to avoid the tails being swamped by accumulated numerical errors. Since the matter field equation and the constraint equations are invariant under reflection symmetry, $w(u, r) \rightarrow \tilde{w}(u, r) := -w(u, r)$, we may specialize to one of the two vacua without loss of generality.

There are a number of different ways to go about solving the Yang-Mills wave equation (6) in Bondi coordinates, e.g. the diamond integral approach due to Gomez and Winicour [9, 10] which we used in [7] or Goldwirth and Piran [11] and Garfinkle's [12] way of rewriting the equation with a total time derivative along the ingoing null geodesics. The latter allows for employing standard *method of lines* (MOL) techniques, i.e. one first discretizes the spatial derivatives (albeit non-equispaced), which in turn,

yields a system of coupled ordinary differential equations (ODEs) that can be solved using a standard ODE solver. In this approach to solving the characteristic initial value problem, the gridpoints usually move along the ingoing null geodesics, which implies a nontrivial origin treatment, with Taylor expansions for increased accuracy.

In contrast to the methods mentioned above, we prefer to simply introduce a new evolution variable

$$h := \bar{w}_{,r} \quad (16)$$

so as to eliminate the mixed ur derivative in equation (6). In addition, we also keep the locations of gridpoints (in time) at fixed values of r . Here, MOL discretizations, using standard stencils for equidistant grids, are applicable and the treatment of the origin is trivial modulo boundary conditions. Moreover, we are here not interested in strong field regions, where the focussing of ingoing null geodesics would provide a natural increase of resolution near the center. Rather, we want to study late time tails for subcritical evolutions, which entails tracking the field at locations of constant r through time.

The evolution equation then becomes

$$\dot{h} = \frac{1}{2} \left(\frac{V}{r} \right)' h + \frac{1}{2} \frac{V}{r} h' - \frac{1}{2} e^{2\beta} \frac{F(\bar{h})}{r^2}, \quad (17)$$

where

$$F(\bar{h}) = 2\bar{h} + 3\bar{h}^2 + \bar{h}^3, \quad (18)$$

and $\bar{h} \equiv \bar{w}$.

We now have an added constraint to solve (in addition to the two geometry equations (10), (11))

$$\bar{h} = \int_0^r h(u, \tilde{r}) d\tilde{r}. \quad (19)$$

Note that equation (17) is of advection type. For flat space and without the YM self-interaction term, it reduces to

$$\dot{h} = \frac{1}{2} h', \quad (20)$$

which is equivalent to the flat space wave equation for

$$\phi = \frac{1}{r} \int_0^r h(u, \tilde{r}) d\tilde{r}. \quad (21)$$

Given initial data $h(u = 0, r) = f(r)$ with $r \in \mathbb{R}$ the solution of the advection equation (20) is simply

$$h(u, r) = f\left(r + \frac{1}{2}u\right), \quad r \in \mathbb{R}, u > 0. \quad (22)$$

The characteristic curves $r + u/2 = \text{const}$ are purely ingoing and thus, there is no boundary condition at the origin of spherical symmetry. The outgoing characteristic of the wave equation comes into play via the constraint equation (21).

The outer boundary needs a different treatment. While it is possible to specify an outgoing wave boundary condition we prefer to use compactification, which has the

advantage of being able to observe late-time behaviour at future null infinity. As in [7] we introduce a compactified radial coordinate

$$x := \frac{r}{1+r}, \quad (23)$$

which maps $r \in [0, \infty] \mapsto x \in [0, 1]$. In addition, we use the Misner-Sharp mass-function

$$m = \frac{r}{2} [1 - g^{rr}] = \frac{r}{2} \left[1 - \frac{V}{r} e^{-2\beta} \right] \quad (24)$$

as an evolution variable, thereby eliminating V . This is necessary, since the compactified constraint equation for V is singular at future null infinity \mathcal{I}^+ , similar to the scalar field case treated in [7]. Instead of h we introduce a new field variable

$$\tilde{h} := \bar{w}_{,x} = \bar{h}_{,x}, \quad (25)$$

which finally leads to a manifestly non-singular evolution system.

The evolution equation then becomes

$$\tilde{h}_u = \frac{1}{2} \left[e^{2\beta} \left(1 - 2m \frac{1-x}{x} \right) (1-x)^2 \tilde{h} \right]_{,x} - \frac{1}{2} e^{2\beta} \frac{F(\bar{h})}{x^2}, \quad (26)$$

and the constraints are

$$\bar{h} = \int_0^x \tilde{h} d\tilde{x} \quad (27)$$

$$\beta_{,x} = \frac{(1-x)^3}{x} (\tilde{h})^2 \quad (28)$$

$$m_{,x} = \left[1 - 2m \frac{1-x}{x} \right] (1-x)^2 (\tilde{h})^2 + \frac{\bar{h}^2 (4 + 4\bar{h} + \bar{h}^2)}{2x^2} \quad (29)$$

The regularity conditions at the origin for the compactified scheme become, using $r = O(x)$,

$$\tilde{h} = O(x) \quad \bar{h} = O(x^2) \quad (30)$$

$$\beta = O(x^2) \quad m = O(x^3) \quad (31)$$

There is no boundary condition at future null infinity, since it is a characteristic.

3. Numerics

From a numerical point of view, we do not even need to know that we are solving a characteristic initial value problem. Rather, we may simply take the evolution system and solve the nonlinear advection equation (26) using a standard MOL approach in conjunction with computing the constraint ODEs (27), (28), and (29).

We may discretize the advection term in (26) by centered, fully upwind or upwind-biased stencils. Combined with an ODE integrator for time, such as, the classical 4th order Runge-Kutta method (RK4), the resulting schemes will then exhibit different numerical errors. One has to make a choice between added dispersion, in the case of centered approximations, and added dissipation for upwind schemes. These errors affect

mostly high frequency components of the solution and can be minimized by using high order approximations.

In the interior of the grid we have chosen a 6th order upwind-biased scheme with the stencil

$$\frac{\partial H}{\partial x}(x_i) = \frac{2H_{i-2} - 24H_{i-1} - 35H_i + 80H_{i+1} - 30H_{i+2} + 8H_{i+3} - H_{i+4}}{60\Delta x} + O(\Delta x^6), \quad (32)$$

where $H_i = H(x_i)$. The above upwind stencil is the one closest to the centered stencil and it also has the lowest error term among the upwind stencils [13]. The two alternate upwind stencils do not lead to stable evolutions in our case. The weights for such finite-difference stencils can conveniently be computed in a computer algebra package, such as Mathematica, using Fornberg's compact algorithm [14]. In contrast to centered schemes, where it is often necessary to add some artificial dissipation to have numerical stability, the dissipation is already "built-in" in our chosen scheme.

The term $F(\bar{h})/x^2$ in (26) forces a regularity boundary condition at the origin, so that

$$\tilde{h}(u, x = 0) = 0. \quad (33)$$

We enforce it by choosing initial data that satisfy this condition (to machine precision) and then make sure that its time derivative is zero, i.e. $\tilde{h}_u(u, x = 0) = 0$ for all timesteps. We choose Gaussian initial data

$$\bar{h}(0, x) = A \exp[-200(x - 1/2)^2]. \quad (34)$$

The constraint equations for \bar{h} and β are integrated using cumulative Newton-Cotes quadrature rules of order 6, which are given in the appendix. Since the right hand side of the constraint equation for the Misner-Sharp mass-function (29) depends on the unknown m , we integrate it with RK4 and use 4th order polynomial interpolation for computing \tilde{h} and \bar{h} at points $x_{i+1/2}$ in between actual gridpoints, as required by the Runge-Kutta method.

In comparison to the established methods for solving characteristic initial value problems [9, 10, 11, 12], the method used here has a number of advantages for the problem at hand. It relies on a standard MOL discretization using equidistant stencils and thus allows for the use of high order schemes. Moreover, the boundary treatment is simple and does not require Taylor series near the origin. It also allows us to track the field at lines of constant r without further interpolation.

In general, we expect the code to be 4th order convergent, see figure 1. For small data, however, $\max 2m/r$ is also small. Since m only appears in the wave equation in this combination, errors in the computation of m may be allowed to be larger than those in other fields, and we may therefore have close to 6th order spatial accuracy, in this case. If the Courant number

$$C := \frac{1}{2} \frac{\Delta u}{\Delta x} \quad (35)$$

is small enough, so that the errors from the RK4 integrator are of order $O(\Delta x^6)$, then, we may in fact achieve 6th order convergence. It is, however, impractical to have small

Courant numbers for very long time evolutions. Clearly, evolutions using high Courant numbers complete faster and need less timesteps than evolutions using lower Courant numbers. Therefore, accumulation errors should also be somewhat less severe for high Courant numbers. Moreover, the classical RK4 solver exhibits additional damping [15] of high frequency modes near the stability limit, which is beneficial to numerical stability.

For weak fields, the Yang-Mills advection equation (26) approximately reduces to

$$\tilde{h}_u = \frac{1}{2}(1-x)^2 \tilde{h}_x. \quad (36)$$

After freezing the nonconstant coefficient $(1-x)^2$ at its maximum 1, Fourier analysis leads to the stability limit (similar to the 6th order centered case discussed in [16])

$$C = \frac{1}{2} \frac{\Delta u}{\Delta x} \leq 1.29 \quad (37)$$

for a MOL discretization with the 6th order upwind-biased stencil (32) and RK4 as time-integrator. For the coupled system, we have found that Courant numbers of up to $C \leq 1.25$ yield stable evolutions.

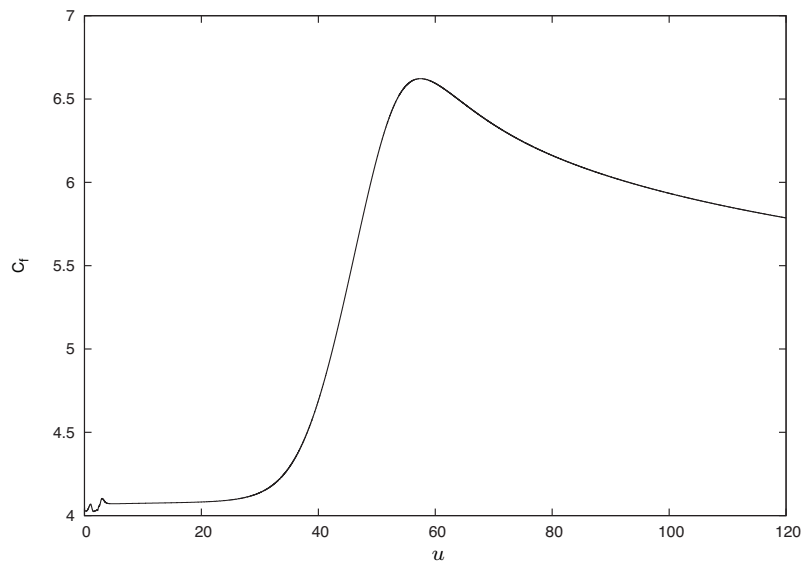


Figure 1. This figure shows the convergence factor $C_f = \log_2 \frac{\|\bar{h}^{1000} - \bar{h}^{500}\|}{\|\bar{h}^{2000} - \bar{h}^{1000}\|}$ in the l_2 -norm of the solution for the coupled EYM-system with grid resolutions of 500, 1000 and 2000 gridpoints and a Courant number of $C = 1.25$. Initially the code is 4th order convergent. Since the initial amplitude $A = 0.28$ is quite large and $2m/r \approx 0.6$ the spatial accuracy is only 4th order. Later in the evolution, as the field disperses, $2m/r$ becomes very small and the spatial discretization becomes roughly 6th order accurate. At even later times the convergence order decreases slowly - probably due to the RK4 time-integrator being the dominant source of errors.

We have used numerical Python to conveniently automate the determination of tail exponents via fitting, while the core of the code was written in C++.

4. Results

Perturbation theory predicts the late-time behaviour of the solution to be

$$\lim_{u \rightarrow \infty} \bar{h}(u, x) = Cu^p, \quad (38)$$

where p is the tail exponent. A first test case for our code is to correctly reproduce the known tail behaviour on Minkowski background [3]. In figure 2 we find that the tail exponent tends to $p = -4$ for observers near timelike infinity i^+ and the exponent $p = -2$ for future null infinity \mathcal{I}^+ . This also corresponds to the decay found on Schwarzschild backgrounds [4]. In terms of the compactified radial coordinate x , the observers are located at $x = (1, 0.9995, 0.999, 0.995, 0.99, 0.95, 0.9, 0.8, 0.7, 0.5)$. For the results presented here, we have used 10000 spatial gridpoints, a Courant number of $C = 1.25$ and an initial data amplitude of $A = 0.01$. For bigger, but still subcritical (in the coupled case), amplitudes and/or smaller Courant numbers, the tail decay is essentially the same.

Figure 3 encodes our main results showing the late-time behavior for the coupled Einstein-Yang-Mills system. We find essentially the same fall-off as for the Yang-Mills field on Minkowski background. As mentioned in the introduction, in terms of a perturbative approach, tails are generated on the one hand by the nonlinearity of the YM field itself, and, on the other by the contribution of the field to the metric. What we see numerically is a superposition of both effects which we can not separate. Hod[17] has studied linear wave tails in time dependent potentials. He finds that for a certain class of potentials that go to zero asymptotically in time, the fall-off behaviour of the tails is a power law depending on the time dependence of the potential.

5. Conclusion

Using Bondi-like coordinates and radial compactification we have written the Einstein-Yang-Mills system as an advection equation plus three constraints. In this form, MOL discretizations are straightforward to apply, the origin treatment is easy and the outer boundary, \mathcal{I}^+ , being a characteristic does not require boundary data. Compared to the diamond integral scheme [9, 10] and Goldwirth, Piran and Garfinkle's [11, 12] way of solving characteristic initial value problems, the approach used here is very clean, simple to implement and allows the use of high order schemes.

We have found that the spherically symmetric coupled Einstein-Yang-Mills system shows the same fall-off behaviour at late times as Yang-Mills on Minkowski or Schwarzschild backgrounds. Although such a result could have been expected it is by no means evident, because so far it is not known how tails arising from the back reaction of the Yang-Mills field to the metric decay. Our results indicate that they decay as fast or faster than the nonlinear tails on Minkowski background.

Our compactified code has allowed us to also study the fall-off behavior at future null infinity. As for the coupled Einstein massless scalar field [7], the fall-off on \mathcal{I}^+ is slower than for observers approaching timelike infinity. Since realistic observers are

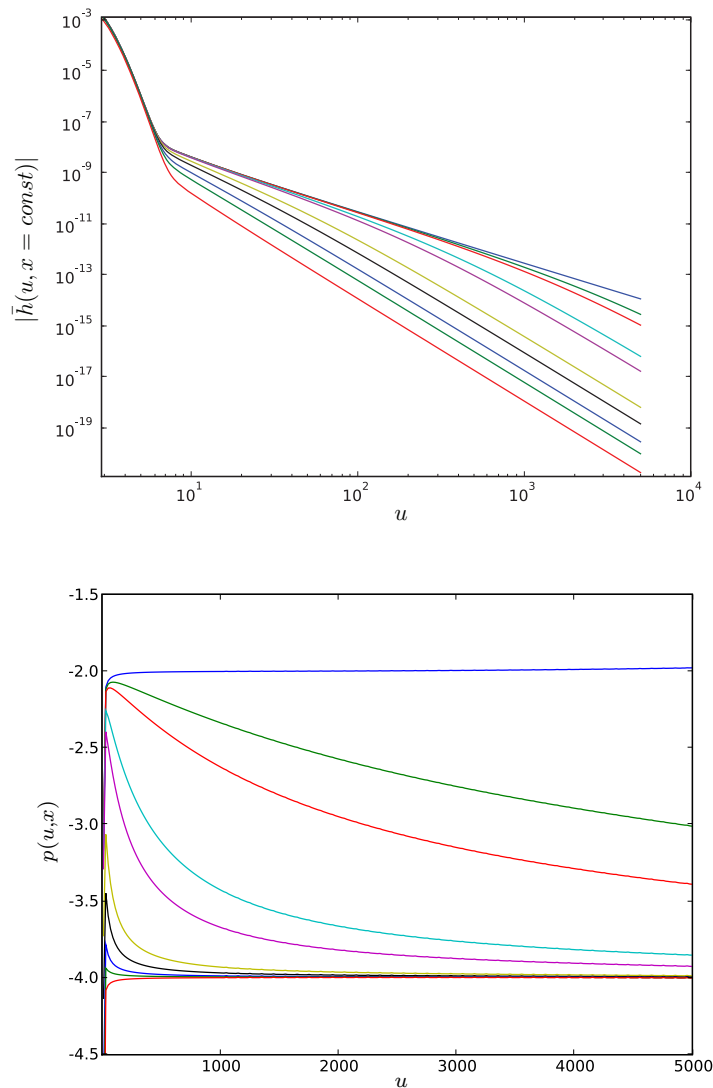


Figure 2. The upper plot shows the decay of the field \bar{h} at $x = \text{const}$ versus retarded time u , while the lower plot depicts the respective tail exponents for the same evolution on Minkowski background. On \mathcal{I}^+ the tail exponent is close to $p = -2$. Observers located at finite x (or r) approach timelike infinity i^+ with the exponent $p = -4$ for late times. Observers closer to the center approach this value faster than those closer to \mathcal{I}^+ .

located only at finite distances from the center, what then is the practical relevance to know the decay conditions on \mathcal{I}^+ ? It has been pointed out in [7] and also in [4], that for astrophysical observers, the relevant decay rate is the one along null infinity. This has to do with the observation that the tail exponents for observers far out start close to the exponent on \mathcal{I}^+ and only slowly decrease to the value for timelike observers.

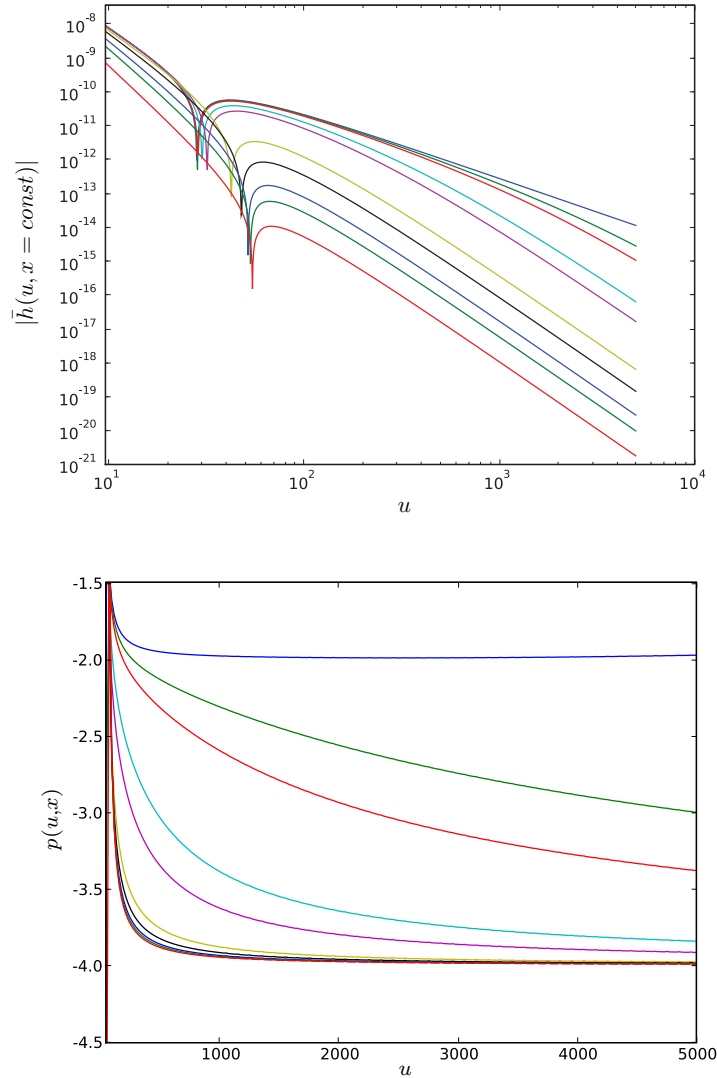


Figure 3. Similar to figure 2 these plots depict the late-time tails and the respective exponents for the coupled Einstein-Yang-Mills system. The exponents coincide with the behaviour on Minkowski space, being $p = -2$ at \mathcal{I}^+ and $p = -4$ at i^+ , respectively. The zero-crossing in \bar{h} at $u \approx 50$ depends on the initial data amplitude, i.e. the field goes through zero earlier for smaller amplitudes.

Acknowledgments

We thank Piotr Bizon for helpful discussions and comments on the manuscript. This work has been supported by the Austrian Fonds zur Förderung der wissenschaftlichen Forschung (FWF) (project P19126-PHY). Partial support by the Fundación Federico is also acknowledged.

Appendix

The quadrature formulas below have been obtained by simply integrating the (quartic) interpolating polynomial $P(f|x_{i-1}, x_i, x_{i+1}, x_{i+2}, x_{i+3})$ on an equidistant grid with spacing h over the intervals $[x_{i-1}, x_i]$ until $[x_{i+2}, x_{i+3}]$, respectively.

$$\int_{x_{i-1}}^{x_i} f dx = \frac{h}{720} (251f_{i-1} + 646f_i - 264f_{i+1} + 106f_{i+2} - 19f_{i+3}) + O(h^7) \quad (\text{A.1})$$

$$\int_{x_i}^{x_{i+1}} f dx = \frac{h}{720} (-19f_{i-1} + 346f_i + 456f_{i+1} - 74f_{i+2} + 11f_{i+3}) + O(h^7) \quad (\text{A.2})$$

$$\int_{x_{i+1}}^{x_{i+2}} f dx = \frac{h}{720} (11f_{i-1} - 74f_i + 456f_{i+1} + 346f_{i+2} - 19f_{i+3}) + O(h^7) \quad (\text{A.3})$$

$$\int_{x_{i+2}}^{x_{i+3}} f dx = \frac{h}{720} (-19f_{i-1} + 106f_i - 264f_{i+1} + 646f_{i+2} + 251f_{i+3}) + O(h^7) \quad (\text{A.4})$$

Summing these formulas together, yields the classical Boole's or Milne's rule.

$$\int_{x_{i-1}}^{x_{i+3}} f dx = \frac{2h}{45} (7f_{i-1} + 32f_i + 12f_{i+1} + 32f_{i+2} + 7f_{i+3}) + O(h^7) \quad (\text{A.5})$$

- [1] Richard H. Price. Nonspherical perturbations of relativistic gravitational collapse. I. Scalar and gravitational perturbations. *Phys. Rev. D*, 5:2419 – 2438, 1972.
- [2] Piotr Bizoń. Huygens' principle and anomalously small radiation tails. *Acta Phys.Polon. B Proc. Supp.*, 1, 2008.
- [3] Piotr Bizoń, Tadeusz Chmaj, and Andrzej Rostworowski. Late-time tails of a yang-mills field on minkowski and schwarzschild backgrounds. *Class. Quant. Grav.*, 24:F55, 2007.
- [4] Anl Zenginoğlu. A hyperboloidal study of tail decay rates for scalar and yang-mills fields. *Class. Quantum Grav.*, 25:175013, 2008.
- [5] Piotr Bizoń. Colored black holes. *Phys. Rev. Lett.*, 64(24):2844, 1990.
- [6] Robert Bartnik and John McKinnon. Particlelike solutions of the Einstein-Yang-Mills equations. *Phys. Rev. Lett.*, 61(2):141, 1988.
- [7] Michael Pürrer, Sascha Husa, and Peter C. Aichelburg. News from critical collapse: Bondi mass, tails, and quasinormal modes. *Phys.Rev. D*, 71(10):104005, 2005.
- [8] Matthew W. Choptuik, Eric W. Hirschmann, and Robert L. Marsa. New critical behavior in einstein-yang-mills collapse. *Phys.Rev. D*, 60:124011, 1999.
- [9] Roberto Gomez and Jeffrey Winicour. Asymptotics of gravitational collapse of scalar waves. *Journal of Mathematical Physics*, 33(4):1445–1457, April 1992.
- [10] Jeffrey Winicour. Characteristic evolution and matching. *Living Reviews in Relativity*, 8(10):39, March 2005.
- [11] Dalia S. Goldwirth and Tsvi Piran. Gravitational collapse of massless scalar field and cosmic censorship. *Physical Review D*, 36(12):3575–3581, December 1987.
- [12] David Garfinkle. Choptuik scaling in null coordinates. *Phys.Rev. D*, 51:5558–5561, 1995.
- [13] Sascha Husa, José A. González, Mark Hannam, Bernd Brügmann, and Ulrich Sperhake. Reducing phase error in long numerical binary black hole evolutions with sixth-order finite differencing. *Class. Quantum Grav.*, 25:105006, 2008.
- [14] Bengt Fornberg. Calculation of weights in finite difference formulas. *SIAM Review*, 40(3):685–691, 1998.
- [15] Dale R. Durran. *Numerical Methods for Wave Equations in Geophysical Fluid Dynamics*. Springer, 1999.

- [16] Bertil Gustafsson, Heinz-Otto Kreiss, and Joseph Oliger. *Time Dependent Problems And Difference Methods*. John Wiley & Sons, Inc., 1995.
- [17] Shahar Hod. *Phys.Rev. D*, 66:024001, 2002.